*Int. J. Therm. Sci.* (2001) 40, 227–244

S1290-0729(00)01213-8/FLA

# Double-diffusive convection in an inclined porous enclosure with opposing temperature and concentration gradients

Ali J. Chamkha *, Hameed Al-Naser

*Department of Mechanical and Industrial Engineering, Kuwait University, P.O. Box 5969, Safat, 13060 Kuwait*

(Received 3 March 2000, accepted 25 May 2000)

**Abstract** — The problem of unsteady, laminar double-diffusive convective flow of a binary gas mixture in an inclined rectangular enclosure filled with a uniform porous medium is considered. Transverse gradients of heat and mass are applied on two opposing walls of the enclosure while the other two walls are adiabatic and impermeable to mass transfer. A numerical solution based on the finite-difference methodology is obtained. In the absence of the porous medium, an oscillatory flow behavior within the enclosure is predicted for a buoyancy ratio of unity. In the presence of the porous medium, however, a decay in the oscillatory behavior is observed. Representative results illustrating the effects of the inverse Darcy number and the enclosure tilting or inclination angle on the contours of streamline, temperature, concentration and density as well as the profiles of velocity, temperature and concentration at mid section of the enclosure are reported. In addition, results for the average Nusselt and Sherwood numbers are presented and discussed for various parametric conditions. In this study, the thermal and the compositional buoyancy forces are assumed to be opposite. © 2001 Éditions scientifiques et médicales Elsevier SAS

**laminar flow / double-diffusive convection / unsteady flow / porous medium / inclined enclosure / numerical analysis / buoyancy**

## Nomenclature

| | | |
|---|---|---|
| $A$ | enclosure aspect ratio $= H/W$ | |
| $c$ | concentration of species | |
| $c_h$ | high species concentration (source) | |
| $c_l$ | low species concentration (sink) | |
| $C$ | dimensionless species concentration $= (c - c_l)/(c_h - c_l) - 0.5$ | |
| $D$ | species diffusivity . . . . . | $m^2 \cdot s^{-1}$ |
| $Da^*$ | Darcy number $= W^2/\kappa$ | |
| $g$ | gravitational acceleration . . . . . | $m \cdot s^{-2}$ |
| $H$ | enclosure height . . . . . | m |
| $Le$ | Lewis number $= \alpha_e/D$ | |
| $N$ | buoyancy ratio $= \beta_c(c_h - c_l)/[\beta_T(T_h - T_c)]$ | |
| $\overline{Nu}$ | average Nusselt number | |
| $p$ | fluid pressure . . . . . | Pa |
| $Pr$ | Prandtl number $= \nu/\alpha_e$ | |
| $Ra_T$ | thermal Rayleigh number $= g\beta_T(T_h - T_c)W^3/(\alpha_e\nu)$ | |
| $\overline{Sh}$ | average Sherwood number | |
| $t$ | time . . . . . | s |
| $t_o$ | period of oscillation . . . . . | s |
| $T$ | temperature . . . . . | K |
| $T_h$ | hot wall temperature (source) . . . . . | K |
| $T_c$ | cold wall temperature (sink) . . . . . | K |
| $u$ | transverse velocity component . . . . . | $m \cdot s^{-1}$ |
| $U$ | dimensionless transverse velocity component $= uW/\alpha_e$ | |
| $v$ | normal velocity component . . . . . | $m \cdot s^{-1}$ |
| $V$ | dimensionless normal velocity component $= vW/\alpha_e$ | |
| $W$ | enclosure width . . . . . | m |
| $x$ | transverse coordinate . . . . . | m |
| $X$ | dimensionless transverse coordinate $= x/W$ | |
| $y$ | normal coordinate . . . . . | m |
| $Y$ | dimensionless normal coordinate $= y/W$ | |

*Greek symbols*

| | |
|---|---|
| $\alpha$ | rectangular enclosure angle |

* Correspondence and reprints.
*E-mail address:* chamkha@kuc01.kuniv.edu.kw (A.J. Chamkha).

| | | |
|---|---|---|
| $\alpha_e$ | effective thermal diffusivity of the porous medium | $m^2 \cdot s^{-1}$ |
| $\beta_T$ | thermal expansion coefficient | $K^{-1}$ |
| $\beta_c$ | compositional expansion coefficient | |
| $\kappa$ | permeability of the porous medium | $m^2$ |
| $\mu$ | dynamic viscosity | $kg \cdot m^{-1} \cdot s^{-1}$ |
| $\nu$ | kinematic viscosity $= \mu/\rho$ | $m^2 \cdot s^{-1}$ |
| $\theta$ | dimensionless temperature $= (T - T_c)/(T_h - T_c) - 0.5$ | |
| $\rho$ | density | $kg \cdot m^{-3}$ |
| $\rho^*$ | dimensionless density $= NC - \theta$ | |
| $\tau$ | dimensionless time $= \alpha_e t / W^2$ | |
| $\tau_o$ | dimensionless period of oscillation $= \alpha_e t_o / W^2$ | |
| $\Omega$ | vorticity | $s^{-1}$ |
| $\psi$ | dimensionless stream function $= \Psi/\alpha_e$ | |
| $\Psi$ | stream function | $m^2 \cdot s^{-1}$ |
| $\zeta$ | dimensionless vorticity $= \Omega W^2/\alpha_e$ | |
| $\nabla^2$ | Laplacian operator | |

## 1. INTRODUCTION

Fluid flows generated by combined temperature and concentration gradients are referred to as double-diffusive convection. The cases of cooperating thermal and concentration buoyancy forces where both forces act in the same direction and opposing thermal and concentration buoyancy forces where both forces act in opposite directions have been considered in the literature. Double diffusion occurs in a wide range of scientific fields such as oceanography, astrophysics, geology, biology and chemical processes (see, for instance, Beghein et al. [1]). Ostrach [2] and Viskanta et al. [3] have reported complete reviews on the subject. Bejan [4] has reported a fundamental study of scale analysis relative to heat and mass transfer within cavities submitted to horizontal combined and pure temperature and concentration gradients. Kamotani et al. [5] have considered an experimental study of natural convection in shallow enclosures with horizontal temperature and concentration gradients. Other experimental studies dealing with thermo-solutal or double-diffusive convection in rectangular enclosures were reported by Ostrach et al. [6] and Lee et al. [7]. Lee and Hyun [8] and Hyun and Lee [9] have reported numerical solutions for unsteady double-diffusive convection in a rectangular enclosure with aiding and opposing temperature and concentration gradients which were in good agreement with reported experimental results. Mamou et al. [10] have reported an analytical and numerical study of double-diffusive convection in a vertical enclosure. Mamou and Vasseur [11] have discussed hysteresis effect on thermosolutal convection with opposed buoyancy forces in inclined enclosures. Other related numerical studies dealing with double-diffusive natural convection in cavities were considered by Ranganathan and Viskanta [12], Trevisan and Bejan [13], Beghein et al. [1] and Nishimura et al. [14].

Thermal buoyancy-induced flow and heat transfer inside a porous medium has been studied extensively in the literature. This is due to its relevance in many natural and industrial processes. This flow situation is induced by a single buoyancy force caused by temperature gradients. Recently, interest for study and analysis of double-diffusive convective flows induced by the combined action of both temperature and concentration gradients has surged in view of its importance in many engineering problems such as migration of moisture contained in fibrous insulation, grain storage, the transport of contaminants in saturated oil, the underground disposal of nuclear wastes and drying processes (Mamou et al. [15]). Chen and Chen [16] have considered double-diffusive fingering convection in a porous medium. Trevisan and Bejan [17] have studied heat and mass transfer by natural convection in a vertical slot filled with a porous medium. Alavyoon [18] has reported on natural convection in vertical porous enclosures due to prescribed fluxes of heat and mass at the vertical boundaries. Mamou et al. [19] have analyzed double-diffusion convection in an inclined slot filled with a porous medium. Lin [20] has studied unsteady natural convection heat and mass transfer in a saturated porous medium. Alavyoon and Masuda [21] have considered natural convection in vertical porous enclosures with opposing fluxes of heat and mass prescribed at the vertical walls. Mamou et al. [15] have studied the onset of double-diffusive convection in an inclined porous enclosure. In their study, Mamou et al. [15] have dealt with a particular situation where the buoyancy forces induced by the thermal and solutal effects were opposing and of equal intensity. The objective of their study was to investigate the critical stability of their system in terms of the inclination angle, aspect ratio and the Lewis number. Double-diffusive convection instability in a vertical porous enclosure has also been analyzed by Mamou et al. [22]. Amahmid et al. [23] have considered boundary layer flows in a vertical porous enclosure induced by opposing forces. More recently, Bennacer et al. [24] have reported on the Brinkman model for thermosolutal convection in a vertical annular porous layer.

In this study, the problem of unsteady, laminar, double-diffusive natural convection flow inside an inclined rectangular enclosure filled with a uniform porous medium with opposing temperature and concentration gradients is

considered for an aspect ratio of 2. This problem represents a direct generalization of the work of Nishimura et al. [14] to include enclosure tilting and porous medium effects and a generalization of the work of Mamou et al. [15] to allow for unequal thermal and concentration buoyancy forces. This type of flow and heat transfer situation finds application in many engineering and technological areas such as geothermal reservoirs, petroleum extraction, chemical catalytic reactors, prevention of sub-soil water pollution, nuclear reactors, underground diffusion of nuclear wastes and other contaminants, and porous material regenerative heat exchangers.

## 2. MATHEMATICAL MODEL

Consider unsteady laminar two-dimensional double-diffusive convective flow inside a tilted fluid-saturated porous medium-filled rectangular enclosure. The temperatures $T_h$ and $T_c$ and concentrations $c_h$ and $c_l$ are uniformly imposed on two opposing walls while the other walls are assumed adiabatic and impermeable to mass transfer. The wall at $T_h$ and $c_h$ is the source where the mixture diffuses to the opposing wall (sink). The schematic of the system under consideration is shown in *figure 1*. The fluid is assumed to be incompressible, Newtonian, and viscous. The viscous dissipation is assumed to be negligible. The Boussinesq approximation with opposite thermal and compositional buoyancy forces is used for the body force terms in the momentum equations.

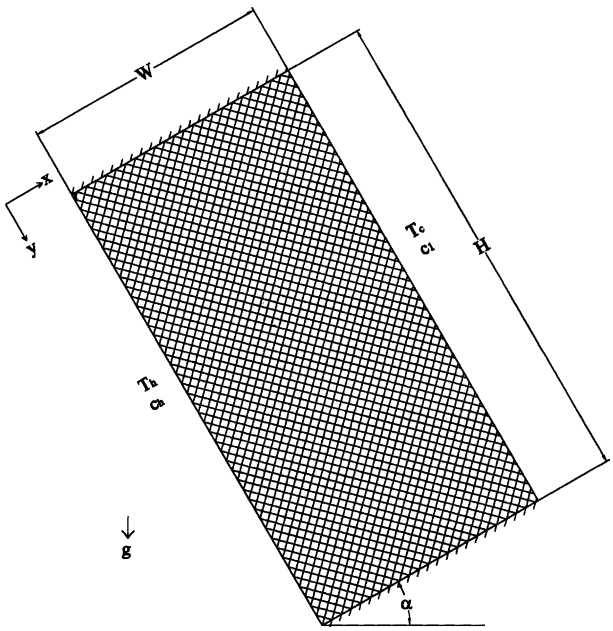


**Figure 1.** Schematic diagram of tilted porous medium filled enclosure.

The governing equations for the problem under consideration are based on the balance laws of mass, linear momentum, thermal energy, and concentration in two dimensions modified to include the Darcian effects of the porous medium. This model is named in the literature as the Darcy–Brinkman model. It is only applicable to slow flows within the enclosure as is typical of many processes such as grain storage and others. Taking into account the assumptions mentioned above, these equations can be written in dimensional form as

$$\frac{\partial u}{\partial x}+\frac{\partial v}{\partial y}=0 \tag{1}$$

$$\frac{\partial u}{\partial t}+u\frac{\partial u}{\partial x}+v\frac{\partial u}{\partial y} =-\frac{1}{\rho}\frac{\partial p}{\partial x}+\nu\left(\frac{\partial^2 u}{\partial x^2}+\frac{\partial^2 u}{\partial y^2}\right)-g\beta_T(T-T_c)\sin\alpha + g\beta_c(c-c_l)\sin\alpha-\frac{\mu}{\rho\kappa}u \tag{2}$$

$$\frac{\partial v}{\partial t}+u\frac{\partial v}{\partial x}+v\frac{\partial v}{\partial y} =-\frac{1}{\rho}\frac{\partial p}{\partial y}+\nu\left(\frac{\partial^2 v}{\partial x^2}+\frac{\partial^2 v}{\partial y^2}\right)-g\beta_T(T-T_c)\cos\alpha + g\beta_c(c-c_l)\cos\alpha-\frac{\mu}{\rho\kappa}v \tag{3}$$

$$\frac{\partial T}{\partial t}+u\frac{\partial T}{\partial x}+v\frac{\partial T}{\partial y}=\alpha_e\left(\frac{\partial^2 T}{\partial x^2}+\frac{\partial^2 T}{\partial y^2}\right) \tag{4}$$

$$\frac{\partial c}{\partial t}+u\frac{\partial c}{\partial x}+v\frac{\partial c}{\partial y}=D\left(\frac{\partial^2 c}{\partial x^2}+\frac{\partial^2 c}{\partial y^2}\right) \tag{5}$$

where $x$, $y$ and $t$ are the transverse and normal distances (as shown on *figure 1*) and time, respectively. $u$, $v$, $p$, $T$ and $c$ are the velocity components in the $x$ and $y$ directions, pressure, temperature and concentration, respectively. $\beta_T$ and $\beta_c$ are the thermal and compositional expansion coefficients, respectively. $\alpha$ is the enclosure angle. $\kappa$, $\alpha_e$, $\nu$, $\mu$, $c_p$, and $\rho$ are the permeability and effective thermal diffusivity of the porous medium, the fluid kinematic and dynamic viscosities, specific heat at constant pressure and the fluid density, respectively. $D$ is the species diffusivity, $T_h$ and $T_c$ are the hot and cold wall temperature, $c_h$ and $c_l$ are the concentration at the hot and cold walls, $g$ is the gravitational acceleration.

The boundary conditions for the problem can be written as

$$\begin{aligned}
&x=0,\ y=y: && u=0,\ v=0,\ T=T_{\mathrm{h}},\ c=c_{\mathrm{h}}\\
&x=W,\ y=y: && u=0,\ v=0,\ T=T_{\mathrm{c}},\ c=c_{\mathrm{l}}\\
&x=x,\ y=0: && u=0,\ v=0,\ \frac{\partial T}{\partial y}=0,\ \frac{\partial c}{\partial y}=0\\
&x=x,\ y=H: && u=0,\ v=0,\ \frac{\partial T}{\partial y}=0,\ \frac{\partial c}{\partial y}=0
\end{aligned} \tag{6}$$

where $W$ and $H$ are the width and height of the enclosure, respectively.

The dimensional stream function and vorticity can be defined in the usual way as

$$u=\frac{\partial \Psi}{\partial y},\qquad v=-\frac{\partial \Psi}{\partial x},\qquad \Omega=-\left(\frac{\partial^2 \Psi}{\partial x^2}+\frac{\partial^2 \Psi}{\partial y^2}\right) \tag{7}$$

Equations (1)–(7) are nondimensionalized using the following dimensionless variables:

$$\begin{aligned}
&\zeta=\frac{\Omega W^2}{\alpha_{\mathrm{e}}},\qquad \psi=\frac{\Psi}{\alpha_{\mathrm{e}}},\qquad \theta=\frac{(T-T_{\mathrm{c}})}{(T_{\mathrm{h}}-T_{\mathrm{c}})}-0.5\\
&C=\frac{(c-c_{\mathrm{l}})}{(c_{\mathrm{h}}-c_{\mathrm{l}})}-0.5,\qquad X=\frac{x}{W}\\
&Y=\frac{y}{W},\qquad \tau=\frac{\alpha_{\mathrm{e}} t}{W^2},\qquad Pr=\frac{\nu}{\alpha_{\mathrm{e}}}\\
&Da^*=\frac{W^2}{\kappa},\qquad N=\frac{\beta_{\mathrm{c}}(c_{\mathrm{h}}-c_{\mathrm{l}})}{\beta_T(T_{\mathrm{h}}-T_{\mathrm{c}})}\\
&Le=\frac{\alpha_{\mathrm{e}}}{D},\qquad Ra_{\mathrm{T}}=\frac{g\beta_T(T_{\mathrm{h}}-T_{\mathrm{c}})W^3}{\alpha_{\mathrm{e}}\nu}
\end{aligned} \tag{8}$$

The meaning of the dimensionless parameters appearing in the above equations is given in the nomenclature list.

By employing equations (8) and combining equations (2) and (3) by eliminating the pressure gradient terms, the resulting dimensionless equations can be written as

$$\zeta=\frac{\partial V}{\partial X}-\frac{\partial U}{\partial Y}=-\nabla^2\psi \tag{9}$$

$$\begin{aligned}
&\frac{\partial \zeta}{\partial \tau}+U\frac{\partial \zeta}{\partial X}+V\frac{\partial \zeta}{\partial Y}\\
&\quad=Pr\nabla^2\zeta+Ra_{\mathrm{T}}Pr\cos\alpha\left(-\frac{\partial \theta}{\partial X}+N\frac{\partial C}{\partial X}\right)\\
&\qquad+Ra_{\mathrm{T}}Pr\sin\alpha\left(\frac{\partial \theta}{\partial Y}-N\frac{\partial C}{\partial Y}\right)-Da^*Pr\zeta
\end{aligned} \tag{10}$$

$$\frac{\partial \theta}{\partial \tau}+U\frac{\partial \theta}{\partial X}+V\frac{\partial \theta}{\partial Y}=\nabla^2\theta \tag{11}$$

$$\frac{\partial C}{\partial \tau}+U\frac{\partial C}{\partial X}+V\frac{\partial C}{\partial Y}=\frac{\nabla^2 C}{Le} \tag{12}$$

The dimensionless boundary conditions become

- $Y=0$:

$$\begin{aligned}
&U=V=\psi=0, && \zeta=-\left(\frac{\partial^2\psi}{\partial Y^2}\right)\\
&\frac{\partial \theta}{\partial Y}=0, && \frac{\partial C}{\partial Y}=0
\end{aligned} \tag{13a}$$

- $Y=H/W$:

$$\begin{aligned}
&U=V=\psi=0, && \zeta=-\left(\frac{\partial^2\psi}{\partial Y^2}\right)\\
&\frac{\partial \theta}{\partial Y}=0, && \frac{\partial C}{\partial Y}=0
\end{aligned} \tag{13b}$$

- $X=0$:

$$\begin{aligned}
&U=V=\psi=0, && \zeta=-\left(\frac{\partial^2\psi}{\partial X^2}\right)\\
&\theta=0.5, && C=0.5
\end{aligned} \tag{13c}$$

- $X=1$:

$$\begin{aligned}
&U=V=\psi=0, && \zeta=-\left(\frac{\partial^2\psi}{\partial X^2}\right)\\
&\theta=-0.5, && C=-0.5
\end{aligned} \tag{13d}$$

The average Nusselt and Sherwood numbers at the source boundary of the enclosure are given by

$$\overline{Nu}=-\int_0^2\frac{\partial \theta}{\partial X}\,\mathrm{d}Y \tag{14}$$

$$\overline{Sh}=-\int_0^2\frac{\partial C}{\partial X}\,\mathrm{d}Y \tag{15}$$

Computations were performed numerically to solve equations (9)–(13) using a 300 MHz PC with the Fortran language. The finite-difference approximation from Taylor series is used to solve the partial differential dimensionless equations with an enclosure aspect ratio of 2. In all the results obtained $Pr=1.0$, $Le=2.0$ and $Ra_{\mathrm{T}}=10^5$ were used as reference values so as to allow for comparisons with the work of Nishimura et al. [14]. A computational domain consisting of $31\times 41$ grid points was used. The details for the numerical algorithm are given below.

## 3. NUMERICAL ALGORITHM

The numerical algorithm used to solve equations (9)–(13) is based on the finite-difference methodology. First,

the central difference is used to approximate the second derivatives and then it is transformed to the implicit line tridiagonal equations and solved in the $x$ direction for the concentration, temperature, vorticity and the stream function. This method was stable and gave results that are very close to the numerical results obtained by Nishimura et al. [14] using the finite-element method.

The finite-difference formulation of equation (9) is

$$\zeta = -\frac{[\psi^{n+1}_{i+1,j} - 2\psi^{n+1}_{i,j} + \psi^{n+1}_{i-1,j}]}{\Delta X^2} - \frac{[\psi^{n}_{i,j+1} - 2\psi^{n+1}_{i,j} + \psi^{n}_{i,j-1}]}{\Delta Y^2} \tag{16a}$$

which can be rearranged as

$$\psi^{n+1}_{i-1,j}[E_1] + \psi^{n+1}_{i,j}[B_1] + \psi^{n+1}_{i+1,j}[A_1] = [D_1] \tag{16b}$$

where

$$\begin{aligned} E_1 &= \left[\Delta Y^2\right] \\ B_1 &= \left[-2\Delta Y^2 - 2\Delta X^2\right] \\ A_1 &= \left[\Delta Y^2\right] \\ D_1 &= -\zeta_{i,j}\Delta X^2 \Delta Y^2 - \Delta X^2\left[\psi^{n}_{i,j+1} + \psi^{n}_{i,j-1}\right] \end{aligned} \tag{16c}$$

The finite-difference formulation for equation (10) will have the form

$$\begin{aligned} &\frac{[\zeta^{n+1}_{i,j} - \zeta^{n}_{i,j}]}{\Delta\tau} + U_{i,j}\frac{[\zeta^{n+1}_{i+1,j} - \zeta^{n+1}_{i-1,j}]}{2\Delta X} + V_{i,j}\frac{[\zeta^{n}_{i,j+1} - \zeta^{n}_{i,j-1}]}{2\Delta Y} \\ &= Pr\left\{\frac{[\zeta^{n+1}_{i+1,j} - 2\zeta^{n+1}_{i,j} + \zeta^{n+1}_{i-1,j}]}{\Delta X^2} + \frac{[\zeta^{n}_{i,j+1} - 2\zeta^{n+1}_{i,j} + \zeta^{n}_{i,j-1}]}{\Delta Y^2}\right\} \\ &+ Ra_T Pr\cos\alpha\left\{-\frac{[\theta_{i+1,j} - \theta_{i-1,j}]}{2\Delta X} + N\frac{[C_{i+1,j} - C_{i-1,j}]}{2\Delta X}\right\} \\ &+ Ra_T Pr\sin\alpha\left\{-\frac{[\theta_{i,j+1} - \theta_{i,j-1}]}{2\Delta Y} - N\frac{[C_{i,j+1} - C_{i,j-1}]}{2\Delta Y}\right\} \\ &- Da^* Pr\,\zeta^{n+1}_{i,j} \end{aligned} \tag{17a}$$

which can be rearranged as

$$\zeta^{n+1}_{i-1,j}[E_1] + \zeta^{n+1}_{i,j}[B_1] + \zeta^{n+1}_{i+1,j}[A_1] = [D_1] \tag{17b}$$

where

$$\begin{aligned} E_1 &= \left[-\frac{U_{i,j}\Delta\tau}{2\Delta X} - \frac{Pr\,\Delta\tau}{\Delta X^2}\right] \\ B_1 &= \left[1.0 + \frac{2Pr\,\Delta\tau}{\Delta X^2} + \frac{2Pr\,\Delta\tau}{\Delta Y^2} + \Delta\tau\, Da^* Pr\right] \\ A_1 &= \left[\frac{U_{i,j}\Delta\tau}{2\Delta X} - \frac{Pr\,\Delta\tau}{\Delta X^2}\right] \\ D_1 &= \zeta^{n}_{i,j+1}\left[-\frac{V_{i,j}\Delta\tau}{2\Delta Y} + \frac{Pr\,\Delta\tau}{\Delta Y^2}\right] \\ &+ \zeta^{n}_{i,j}[1.0] + \zeta^{n}_{i,j-1}\left[\frac{V_{i,j}\Delta\tau}{2\Delta Y} + \frac{Pr\,\Delta\tau}{\Delta Y^2}\right] \\ &+ Ra_T Pr\,\Delta\tau\cos\alpha\left\{-\frac{[\theta_{i+1,j} - \theta_{i-1,j}]}{2\Delta X} + N\frac{[C_{i+1,j} - C_{i-1,j}]}{2\Delta X}\right\} \\ &+ Ra_T Pr\,\Delta\tau\sin\alpha\left\{-\frac{[\theta_{i,j+1} - \theta_{i,j-1}]}{2\Delta Y} - N\frac{[C_{i,j+1} - C_{i,j-1}]}{2\Delta Y}\right\} \end{aligned} \tag{17c}$$

The finite-difference formulation for equation (11) will be written as

$$\begin{aligned} &\frac{[\theta^{n+1}_{i,j} - \theta^{n}_{i,j}]}{\Delta\tau} + U_{i,j}\frac{[\theta^{n+1}_{i+1,j} - \theta^{n+1}_{i-1,j}]}{2\Delta X} + V_{i,j}\frac{[\theta^{n}_{i,j+1} - \theta^{n}_{i,j-1}]}{2\Delta Y} \\ &= \left\{\frac{[\theta^{n+1}_{i+1,j} - 2\theta^{n+1}_{i,j} + \theta^{n+1}_{i-1,j}]}{\Delta X^2} + \frac{[\theta^{n}_{i,j+1} - 2\theta^{n}_{i,j} + \theta^{n}_{i,j-1}]}{\Delta Y^2}\right\} \end{aligned} \tag{18a}$$

which can be rearranged as

$$\theta^{n+1}_{i-1,j}[E_1] + \theta^{n+1}_{i,j}[B_1] + \theta^{n+1}_{i+1,j}[A_1] = [D_1] \tag{18b}$$

where

$$\begin{aligned} E_1 &= \left[-\frac{U_{i,j}\Delta\tau}{2\Delta X} - \frac{\Delta\tau}{\Delta X^2}\right] \\ B_1 &= \left[1.0 + \frac{2\Delta\tau}{\Delta X^2}\right] \end{aligned}$$

$$A_1 = \left[\frac{U_{i,j}\Delta\tau}{2\Delta X} - \frac{\Delta\tau}{\Delta X^2}\right]$$
$$D_1 = \theta^n_{i,j+1}\left[-\frac{V_{i,j}\Delta\tau}{2\Delta Y} + \frac{\Delta\tau}{\Delta Y^2}\right] + \theta^n_{i,j}\left[1.0 - \frac{2\Delta\tau}{\Delta Y^2}\right] + \theta^n_{i,j-1}\left[\frac{V_{i,j}\Delta\tau}{2\Delta Y} + \frac{\Delta\tau}{\Delta Y^2}\right] \quad (18c)$$

The finite-difference formulation for equation (12) can be written as

$$\frac{[C^{n+1}_{i,j} - C^n_{i,j}]}{\Delta\tau} + U_{i,j}\frac{[C^{n+1}_{i+1,j} - C^{n+1}_{i-1,j}]}{2\Delta X} + V_{i,j}\frac{[C^n_{i,j+1} - C^n_{i,j-1}]}{2\Delta Y} = \frac{1}{Le}\left\{\frac{[C^{n+1}_{i+1,j} - 2C^{n+1}_{i,j} + C^{n+1}_{i-1,j}]}{\Delta X^2} + \frac{[C^n_{i,j+1} - 2C^n_{i,j} + C^n_{i,j-1}]}{\Delta Y^2}\right\} \quad (19a)$$

which can be rearranged as

$$C^{n+1}_{i-1,j}[E_1] + C^{n+1}_{i,j}[B_1] + C^{n+1}_{i+1,j}[A_1] = [D_1] \quad (19b)$$

where

$$E_1 = \left[-\frac{U_{i,j}\Delta\tau}{2\Delta X} - \frac{\Delta\tau}{Le\,\Delta X^2}\right]$$
$$B_1 = \left[1.0 + \frac{2\Delta\tau}{Le\,\Delta X^2}\right]$$
$$A_1 = \left[\frac{U_{i,j}\Delta\tau}{2\Delta X} - \frac{\Delta\tau}{Le\,\Delta X^2}\right]$$
$$D_1 = C^n_{i,j+1}\left[-\frac{V_{i,j}\Delta\tau}{2\Delta Y} + \frac{\Delta\tau}{Le\Delta Y^2}\right] + C^n_{i,j}\left[1.0 - \frac{2\Delta\tau}{Le\,\Delta Y^2}\right] + C^n_{i,j-1}\left[\frac{V_{i,j}\Delta\tau}{2\Delta Y} + \frac{\Delta\tau}{Le\,\Delta Y^2}\right] \quad (19c)$$

$U$ and $V$ can be determined explicitly from

$$U^{n+1}_{i,j} = \frac{[\psi_{i,j+1} - \psi_{i,j-1}]}{2\Delta Y}$$
$$V^{n+1}_{i,j} = -\frac{[\psi_{i+1,j} - \psi_{i-1,j}]}{2\Delta X} \quad (20)$$

The finite-difference formulation for the boundary condition (13) is:

- $Y = 0$:

$$\zeta = -\left(\frac{\partial^2\psi}{\partial Y^2}\right) \Rightarrow \zeta^{n+1}_{i,1} = -\frac{[2\psi^n_{i,1} - 5\psi^n_{i,2} + 4\psi^n_{i,3} - \psi^n_{i,4}]}{\Delta Y^2} \quad (21)$$
$$\frac{\partial\theta}{\partial Y} = 0 \Rightarrow \theta^{n+1}_{i,1} = \frac{[4\theta^n_{i,2} - \theta^n_{i,3}]}{3.0} \quad (22)$$
$$\frac{\partial C}{\partial Y} = 0 \Rightarrow C^{n+1}_{i,1} = \frac{[4C^n_{i,2} - C^n_{i,3}]}{3.0} \quad (23)$$

- $Y = H/W$:

$$\zeta = -\left(\frac{\partial^2\psi}{\partial Y^2}\right) \Rightarrow \zeta^{n+1}_{i,j_{\max}} = -[-\psi^n_{i,j_{\max}-3} + 4\psi^n_{i,j_{\max}-2} - 5\psi^n_{i,j_{\max}-1} + 2\psi^n_{i,j_{\max}}]/\Delta Y^2 \quad (24)$$
$$\frac{\partial\theta}{\partial Y} = 0 \Rightarrow \theta^{n+1}_{i,j_{\max}} = \frac{[4\theta^n_{i,j_{\max}-1} - \theta^n_{i,j_{\max}-2}]}{3.0} \quad (25)$$
$$\frac{\partial C}{\partial Y} = 0 \Rightarrow C^{n+1}_{i,j_{\max}} = \frac{[4C^n_{i,j_{\max}-1} - C^n_{i,j_{\max}-2}]}{3.0} \quad (26)$$

- $X = 0$:

$$\zeta = -\left(\frac{\partial^2\psi}{\partial X^2}\right) \Rightarrow \zeta^{n+1}_{1,j} = 2\frac{[\psi^n_{1,j} - \psi^n_{2,j}]}{\Delta X^2} \quad (27)$$
$$\theta^{n+1}_{1,j} = 0.5, \qquad C^{n+1}_{1,j} = 0.5 \quad (28)$$

- $X = 1$:

$$\zeta = -\left(\frac{\partial^2\psi}{\partial X^2}\right) \Rightarrow \zeta^{n+1}_{i_{\max},j} = 2\frac{[\psi^n_{i_{\max},j} - \psi^n_{i_{\max}-1,j}]}{\Delta X^2} \quad (29)$$
$$\theta^{n+1}_{i_{\max},j} = -0.5, \qquad C^{n+1}_{i_{\max},j} = -0.5 \quad (30)$$

The subscripts $i$ and $j$ denote the $X$ and $Y$ location. The superscripts $n$ and $n+1$ denote the time step, respectively. The numerical computations are carried out for $31 \times 41$ grid nodal points for a time step of $10^{-5}$, $\Delta X = 1/30$ and $\Delta Y = 1/20$. The convergence criterion required that the difference between the current and previous iterations for all of the dependent variables be $10^{-4}$.

## 4. SOLUTION PROCEDURE

1. All dependent variables are initialized to zero.

2. The new boundary condition values at $(n+1)$ are calculated for all walls from the previous values at $(n)$.

3. The new concentration values at $(n+1)$ are calculated from the previous $(n)$ values, and then a subroutine is called to solve the obtained tridiagonal equations for all the concentration values at all the internal grid points.

4. The temperature, vorticity, and the stream function are calculated in the same way as in step (3), respectively.

5. The velocity components $U$ and $V$ are calculated at $(n+1)$ from the values at $(n)$ explicitly for all the internal grid points.

6. The error is calculated for the concentration, the temperature, and the vorticity at the last time step (only for steady solution).

7. To obtain the solution at the next time step at $(n+2)$, the same procedure is followed by starting with step (2).

This procedure is for unsteady solution. If the steady solution is required, then the concentration and the temperature are only needed to be updated for a number of internal loops for each single time step. Then, at the end of this single time step, the vorticity, the stream function, and the velocity components ($U$ and $V$) need to be updated.

8. The average Nusselt and Sherwood numbers are then calculated at the source wall.

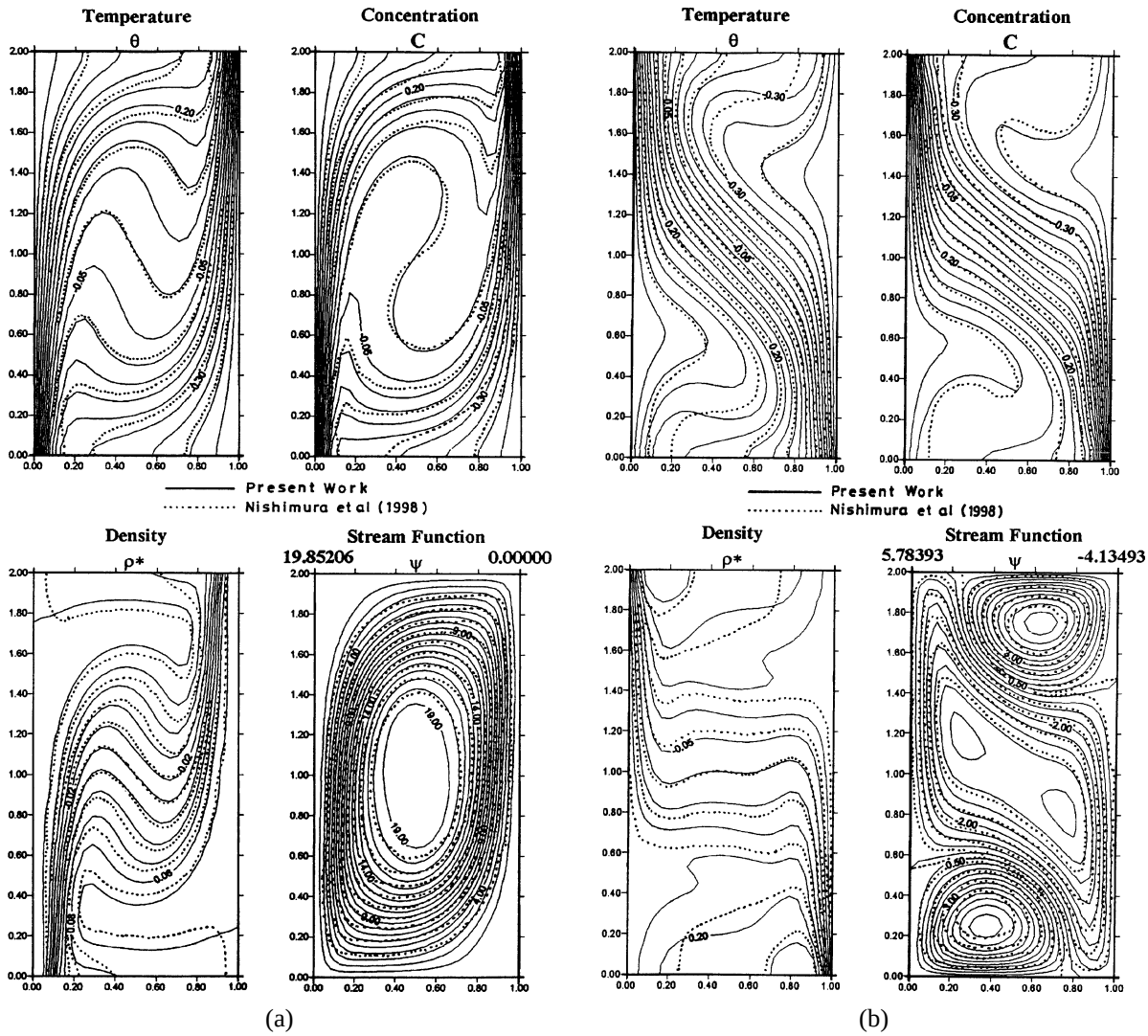


**Figure 2.** (a) Steady thermal-dominated solution for $N = 0.8$, $Da = 0.0$, $\alpha = 0.0$. (b) Steady compositional-dominated solution for $N = 1.3$, $Da = 0.0$, $\alpha = 0.0$.

## 5. NUMERICAL VALIDATION TESTS

In order to check the accuracy of the numerical method employed for the solution of the problem under consideration, it was validated against the problem of double-diffusive convective flow in a vertical rectangular enclosure with combined horizontal temperature and concentration gradients reported earlier by Nishimura et al. [14]. *Figure 2* presents comparison for the streamlines, isotherms, concentration contours and density contours of the present work at $N = 0.8$ (thermal-dominated flow) and $N = 1.3$ (compositional-dominated flow) with those of Nishimura et al. [14]. This comparison shows good agreement between the results. *Figure 3* illustrates the oscillatory behavior in $|\psi_{\max}|$ and $|\psi_{\min}|$ with time predicted by Nishimura et al. [14]. The period of oscillation $\tau_o$ was found to be 0.05091. Also, *figures 4a–d* corresponding to points *a–d* in *figure 3*, respectively, predict the oscillatory behavior with time in the thermal and compositional recirculations at $N = 1.0$ through the streamline, temperature, concentration and density contours which compare well with the results reported by Nishimura et al. [14]. Moreover, *table I* shows a favorable comparison between numerical results for a period of oscillation and stream function extrema $|\psi_{\max}|$ and $|\psi_{\min}|$ at $N = 1.0$ obtained by three different numerical schemes, the finite-element method, spectral method (reported by Nishimura et al. [14]) and the finite-difference method of the present work. These various comparisons lend confidence in the numerical results to be reported subsequently.

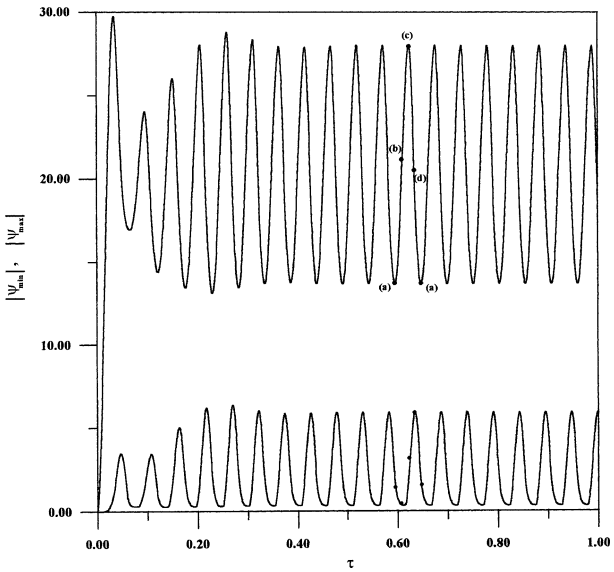


**Figure 3.** Oscillatory behavior of $|\psi_{\min}|$ and $|\psi_{\max}|$ with time for $N = 1.0$, $Da^* = 0.0$, $\alpha = 0°$.

## 6. RESULTS AND DISCUSSION

In this section, numerical results for the streamline, temperature, concentration and density contours as well as selected velocity, temperature and concentration profiles at mid-section of the enclosure for various values of the enclosure inclination angle $\alpha$ and inverse Darcy number $Da^*$ will be reported. In addition, representative results for the average Nusselt number $\overline{Nu}$ and the average Sherwood number $\overline{Sh}$ at various conditions will be presented and discussed. In all of these results, *Le*, *Pr*, and $Ra_T$ were fixed at the values of 2.0, 1.0 and $10^5$, respectively.

*Figure 5* presents steady-state contours for the streamline, temperature, concentration, and density at various values of the enclosure inclination angle $\alpha$ for $Da^* = 0.0$ and $N = 0.8$. As mentioned by Nishimura et al. [14], when $N < 1.0$ the flow is primarily dominated by thermal buoyancy effects while for $N > 1.0$ the flow is mainly dominated by compositional buoyancy effects. The interaction between the thermal and compositional buoy-

TABLE I
Comparison between the present method and two numerical methods for $N = 1.0$.

| | Finite element method ($31 \times 41$ points) [14] | Spectral method ($40 \times 80$ points) [25] | Finite difference method ($31 \times 41$ points) Present results |
|---|---|---|---|
| $\tau_o$ | 0.0497 | 0.0494 | 0.05091 |
| Max $\|\psi_{\max}\|$ | 26.7 | 26.8 | 27.8 |
| Min $\|\psi_{\max}\|$ | 12.9 | 12.7 | 13.7 |
| Max $\|\psi_{\min}\|$ | 5.76 | 5.52 | 5.85 |
| Min $\|\psi_{\min}\|$ | 0.351 | 0.333 | 0.333 |

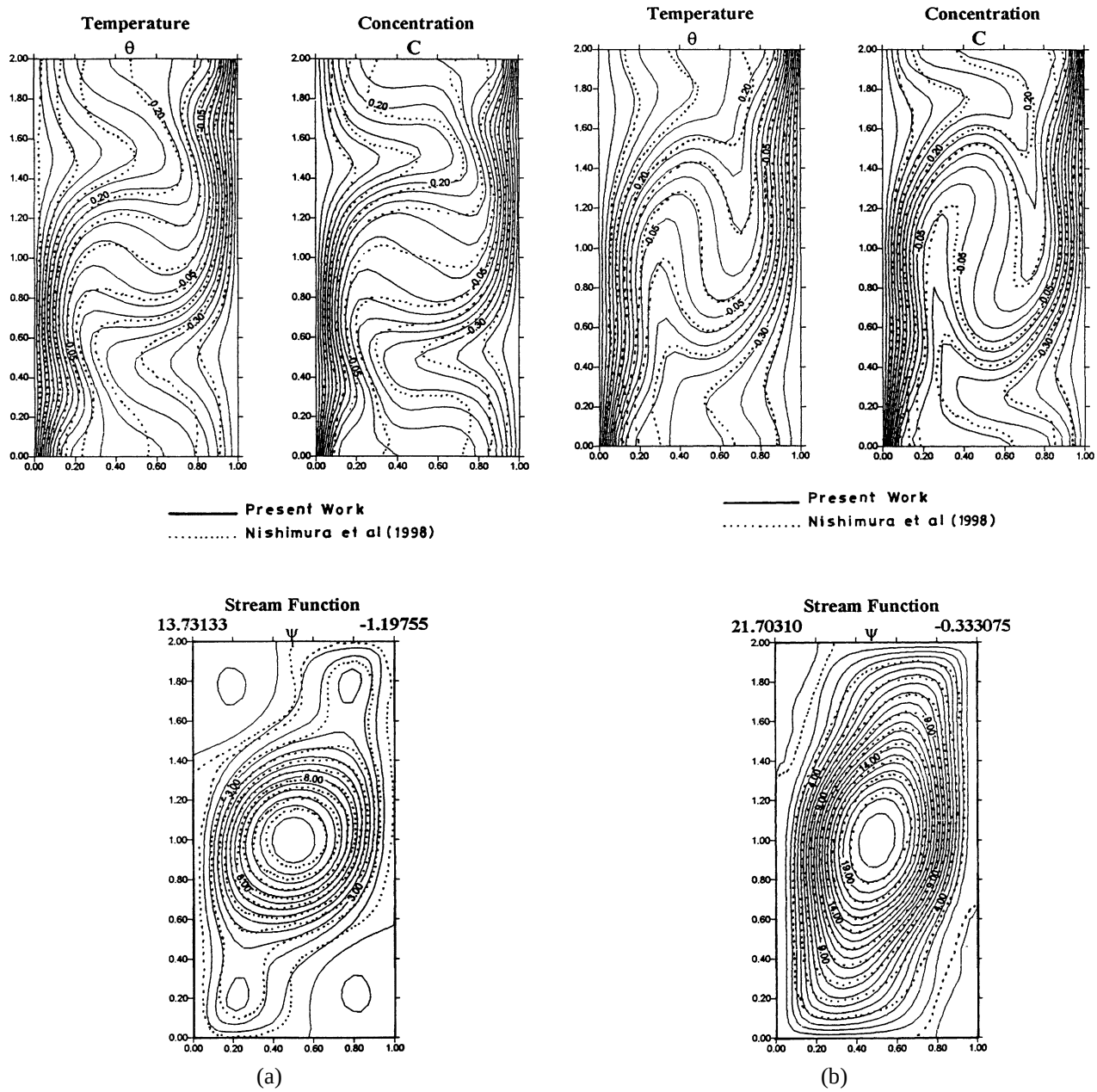


**Figure 4.** Temperature, concentration, density and streamline contours during a period of oscillation (a) for $N = 1.0$, $Da = 0.0$, $\alpha = 0.0$. (b) for $N = 1.0$, $Da = 0.0$, $\alpha = 0.0$. Temperature, concentration, density and streamline contours during a period of oscillation (c) for $N = 1.0$, $Da = 0.0$, $\alpha = 0.0$. (d) for $N = 1.0$, $Da = 0.0$, $\alpha = 0.0$.

ancy effects is small except for values of $N$ close to unity. Therefore, for $N = 0.8$, the thermal buoyancy dominates and a large clockwise thermal recirculation is predicted with the isotherms not being horizontally uniform in the core region within the enclosure. Furthermore, the concentration contours are distorted in the core of the enclosure while the density contours indicate a stable stratification in the vertical direction except near the insulated walls of the enclosure. As the enclosure is tilted, the streamline contours are distorted with the maximum value of the stream function occurring for $\alpha = 0^\circ$ which indicates a faster clockwise thermal recirculation than

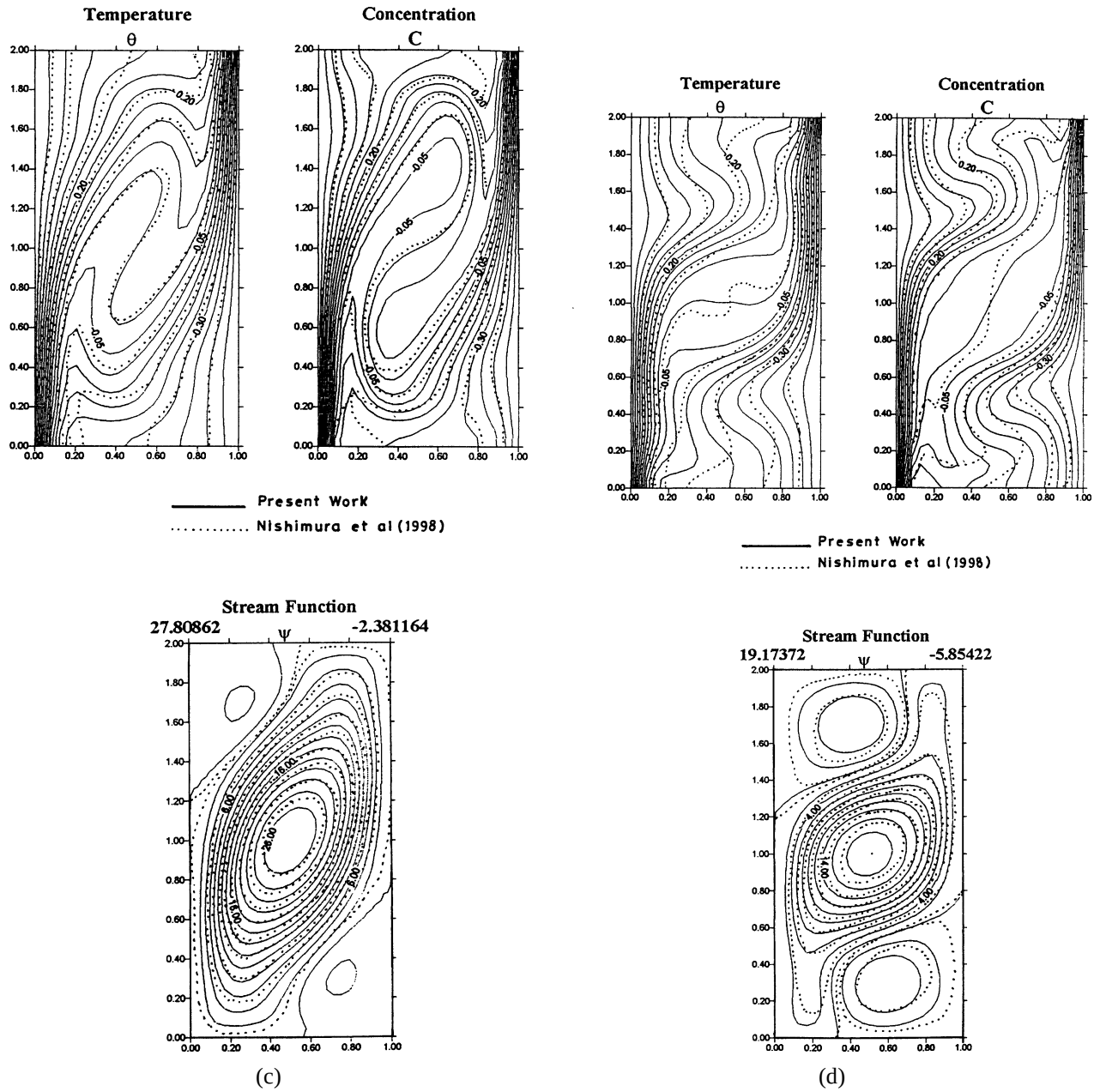


**Figure 4** (continued).

that of a higher inclination angle. The temperature and density contours become more horizontally uniform in the core region within the enclosure for $\alpha = 30°$. In addition, the concentration contours become less distorted as $\alpha$ increases.

*Figure 6* displays similar results as shown in *figure 5* except for $N = 1.3$. As mentioned before, for this specific value of $N$, the flow is dominated by compositional buoyancy effects. For $\alpha = 0°$ a counter-clockwise compositional recirculation exists in the core region of the enclosure along with two clockwise thermal recirculations occurring near the top right and bottom left corners of the enclosure. The contours for temperature and concentration are almost parallel to each other within the cen-

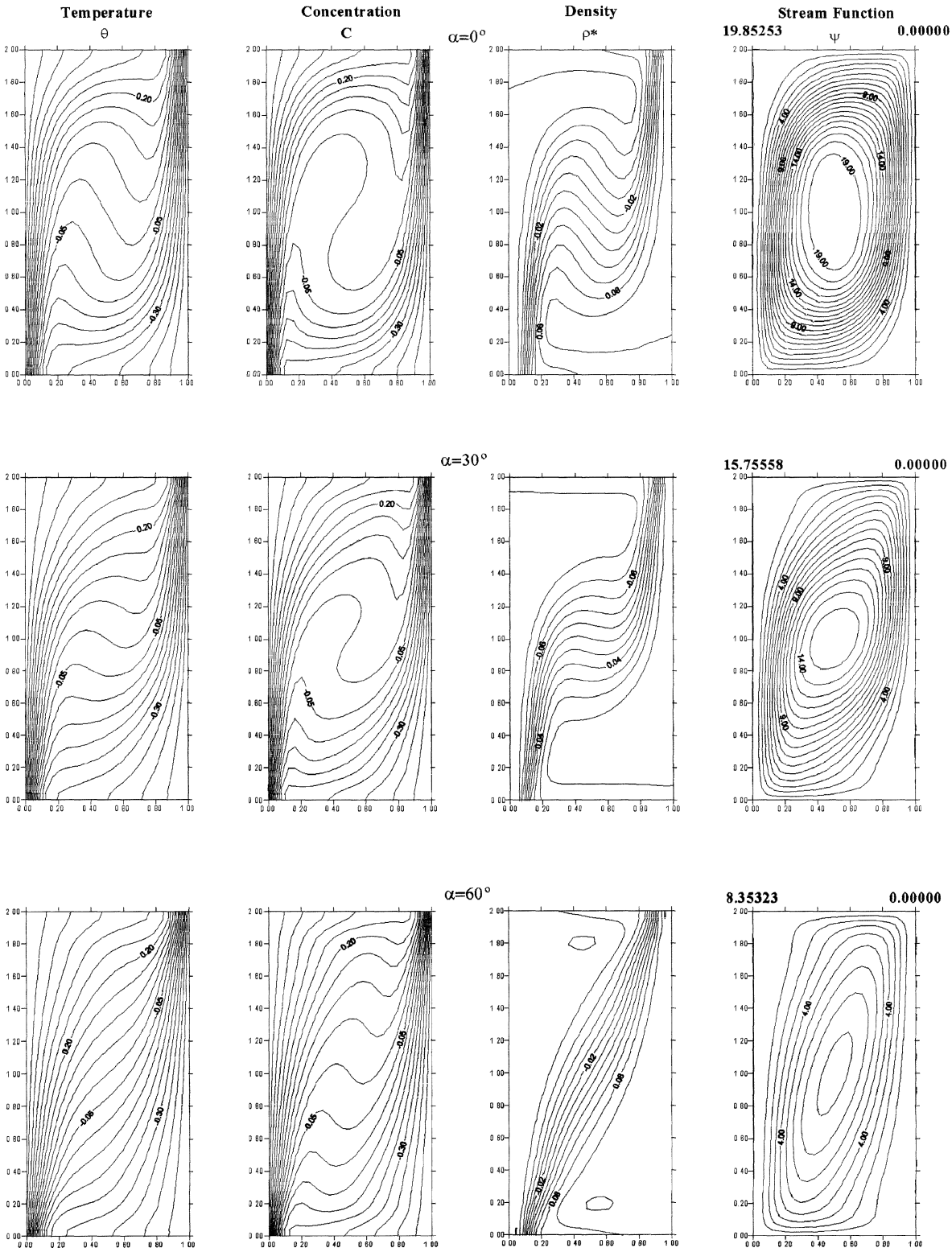


**Figure 5.** Steady thermal-dominated solution for $Da^* = 0.0$, $Le = 2.0$, $N = 0.8$, $Pr = 1.0$, and $Ra_T = 10^5$.

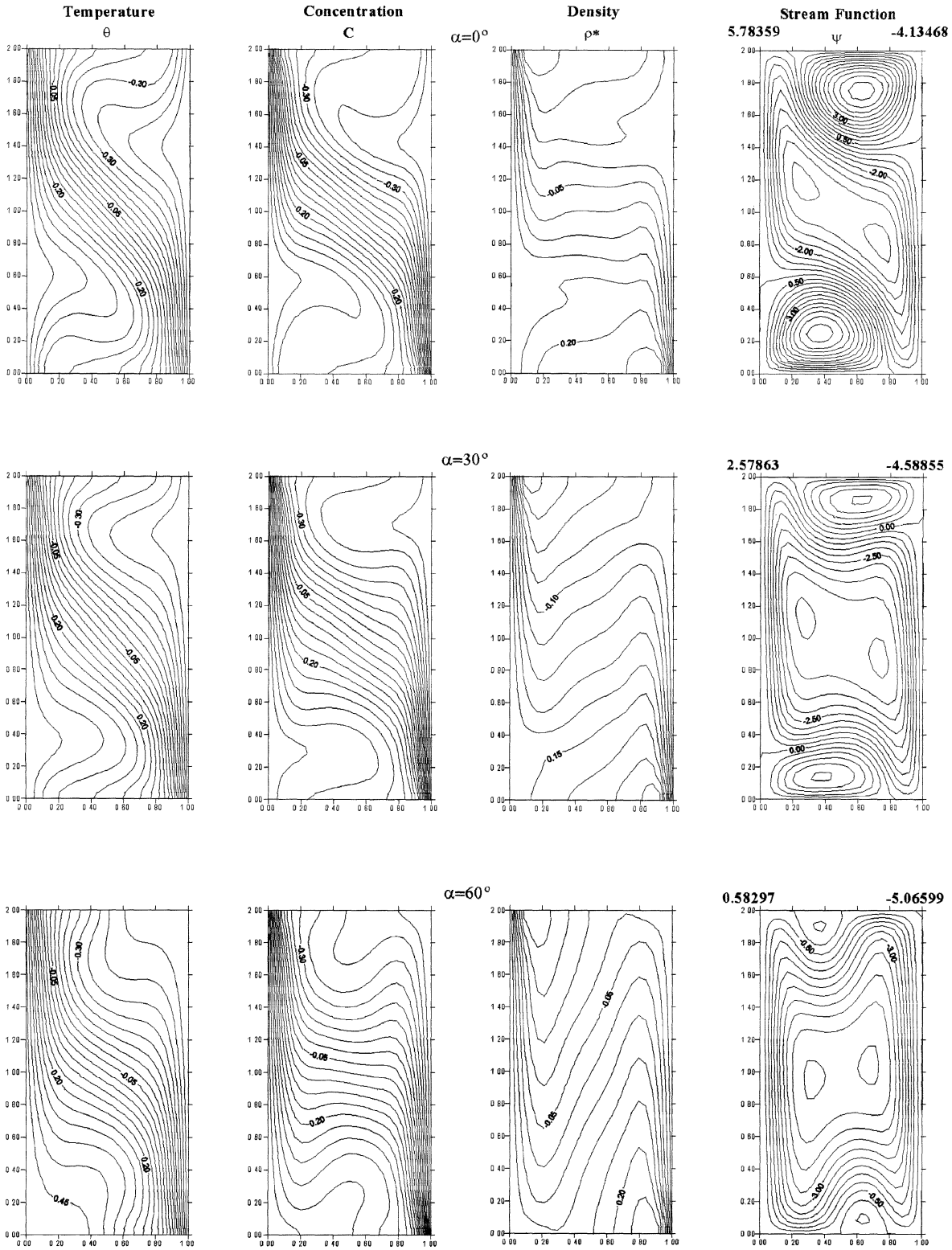


**Figure 6.** Steady compositional-dominated solution for $Da^* = 0.0$, $Le = 2.0$, $N = 0.8$, $Pr = 1.0$, and $Ra_T = 10^5$.

ter of the enclosure away from the walls which produces a more horizontally uniform density contours which are stably stratified in the vertical direction. However, as the inclination angle $\alpha$ increases further and further, the two thermal recirculations at the corners diminish while the compositional recirculation dominates and moves slower in the core region of the enclosure. Also, the temperature and concentration contours become less parallel to each other within the core, and thus, the density contours become less horizontally uniform. In this case, the density remains stably stratified in the vertical direction. An inspection of the maximum value of the stream function for $\alpha = 0°$, 30°, and 60° reveals that it is the highest for $\alpha = 0°$ and decreases as $\alpha$ increases. This indicates that the flow behavior is fastest at $\alpha = 0°$ and becomes slower as $\alpha$ increases.

*Figure 7* depicts the effects of the inverse Darcy number $Da^*$ on the flow, thermal and compositional patterns within the enclosure through the streamline, temperature, concentration and density contours for a buoyancy ratio $N = 0.8$. The presence of the porous medium is observed to cause the streamlines to be distorted with the formation of a smaller thermal and slower clockwise recirculation in the core region. The temperature and concentration contours tend to become more similar except in the core region as $Da^*$ increases causing the density contours to become less horizontally uniform in the core region away from the walls of the enclosure. A main contribution of the presence of the porous medium for this buoyancy ratio is seen to provide flow resistance and to suppress the overall heat transfer in the enclosure.

In *figure 8*, similar results as those shown in *figure 7* are displayed for $N = 1.3$ (compositional-dominated flow). Similar trends in the flow patterns are predicted where the two clockwise thermal recirculations and the compositional recirculation are slowed down by the presence of the porous medium. The temperature and concentration contours appear to look more similar while the density contours become more horizontally uniform in the core region as $Da^*$ increases.

Representative profiles at mid-section of the enclosure for the $X$-component of velocity $U$, $Y$-component of velocity $V$, temperature $\theta$, and concentration $C$ for various values of $\alpha$ and $Da^*$ for $N = 0.8$ were obtained but not presented herein for brevity. It was predicted from these results that as $\alpha$ was increased from 0 to 30° and then to 60°, all of $V$, $\theta$, and $C$ increased in the vicinity of the hot wall while $U$ increased reaching a maximum for $\alpha = 30°$ and then decreased for $\alpha = 60°$. This is believed to be associated with the oscillatory behavior inherent in the problem as was observed from the curve associated with $\alpha = 0°$.

A very similar behavior as that of $\alpha$ was observed for all profiles where $V$, $\theta$, and $C$ near the hot wall increased with increasing values of $Da^*$ ($Da^* = 0$, 100, 200, 300, 500) while $U$ increased reaching a maximum for $Da^* = 100$ and then decreased for values of $Da^* > 100$. The oscillatory behavior of $U$ for $Da^* = 0$ was predicted to disappear as $Da^*$ was increased.

Another typical set of profiles for $U$, $V$, $\theta$, and $C$ for various values of $\alpha$ and $Da^*$ at mid-section of the enclosure for $N = 1.3$ was also obtained. In many of these results, the exact opposite behavior reported for the case of $N = 0.8$ was observed. In fact, the profiles of $U$, $\theta$ and $C$ at the hot wall decreased while the profiles of $V$ increased as the enclosure inclination angle was increased. The behaviors of $U$, $\theta$ and $C$ were in contrast with their counterparts for $N = 0.8$.

Furthermore, a resistive behavior of the flow with a slight increase in both the temperature and concentration due to the presence of the porous medium was clearly predicted as $Da^*$ was increased. The behaviors of $U$ and $V$ for this case were in contrast with their counterparts for $N = 0.8$. Also, as opposed to the case of $N = 0.8$, no oscillatory behavior in the profile of $U$ is predicted for $Da^* = 0$.

The effects of the enclosure inclination angle $\alpha$ and the inverse Darcy number $Da^*$ on the average Nusselt number $\overline{Nu}$ and the average Sherwood number $\overline{Sh}$ for a buoyancy ratio $N = 0.8$ are presented in *figures 9* and *10*, respectively. It is observed that both of $\overline{Nu}$ and $\overline{Sh}$ have a decreasing trend with increases in $Da^*$. In addition, tilting the enclosure has the tendency to decrease the temperature and concentration gradients at the hot wall resulting in reductions in both $\overline{Nu}$ and $\overline{Sh}$ as clearly shown in *figures 9* and *10*.

A similar set of results for $\overline{Nu}$ and $\overline{Sh}$ as those reported in *figures 9* and *10* are illustrated in *figures 11* and *12* for $N = 1.3$. In these figures, it is interesting to observe that tilting the enclosure produces the opposite behavior as compared with those corresponding to $N = 0.8$. Namely, $\overline{Nu}$ and $\overline{Sh}$ tend to increase as $\alpha$ increases for $N = 1.3$.

*Figures 13* and *14* illustrate the influence of the buoyancy ratio $N$ on the average Nusselt and Sherwood numbers for various values of $Da^*$. An interesting behavior in both of these figures is predicted in which $\overline{Nu}$ and $\overline{Sh}$ are minimum for the critical buoyancy ratio of 1.2. This is true regardless of the value of the inverse Darcy number.

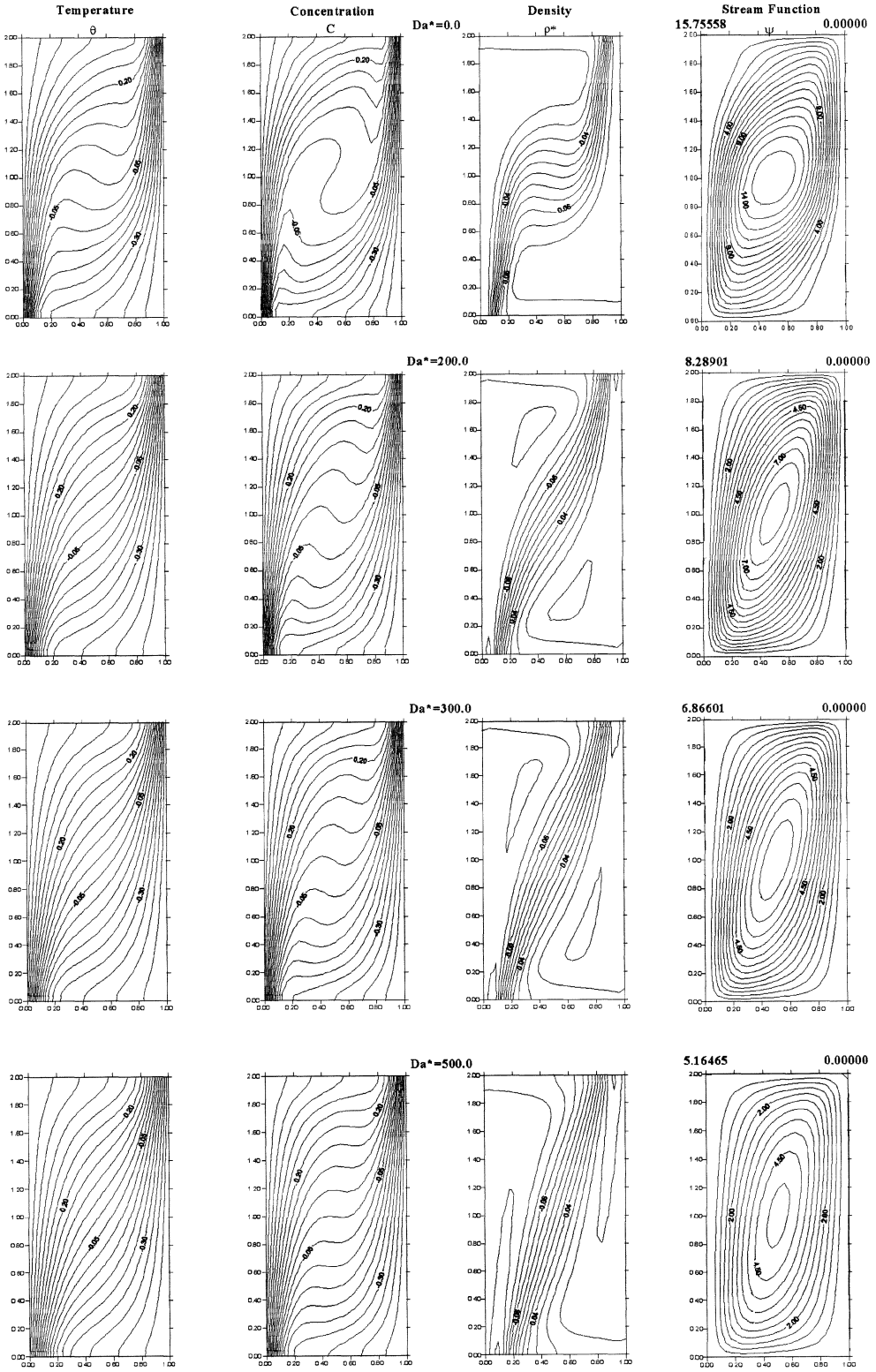


**Figure 7.** Steady thermal-dominated solution for $Le = 2.0$, $N = 0.8$, $Pr = 1.0$, $Ra_T = 10^5$, and $\alpha = 30°$.

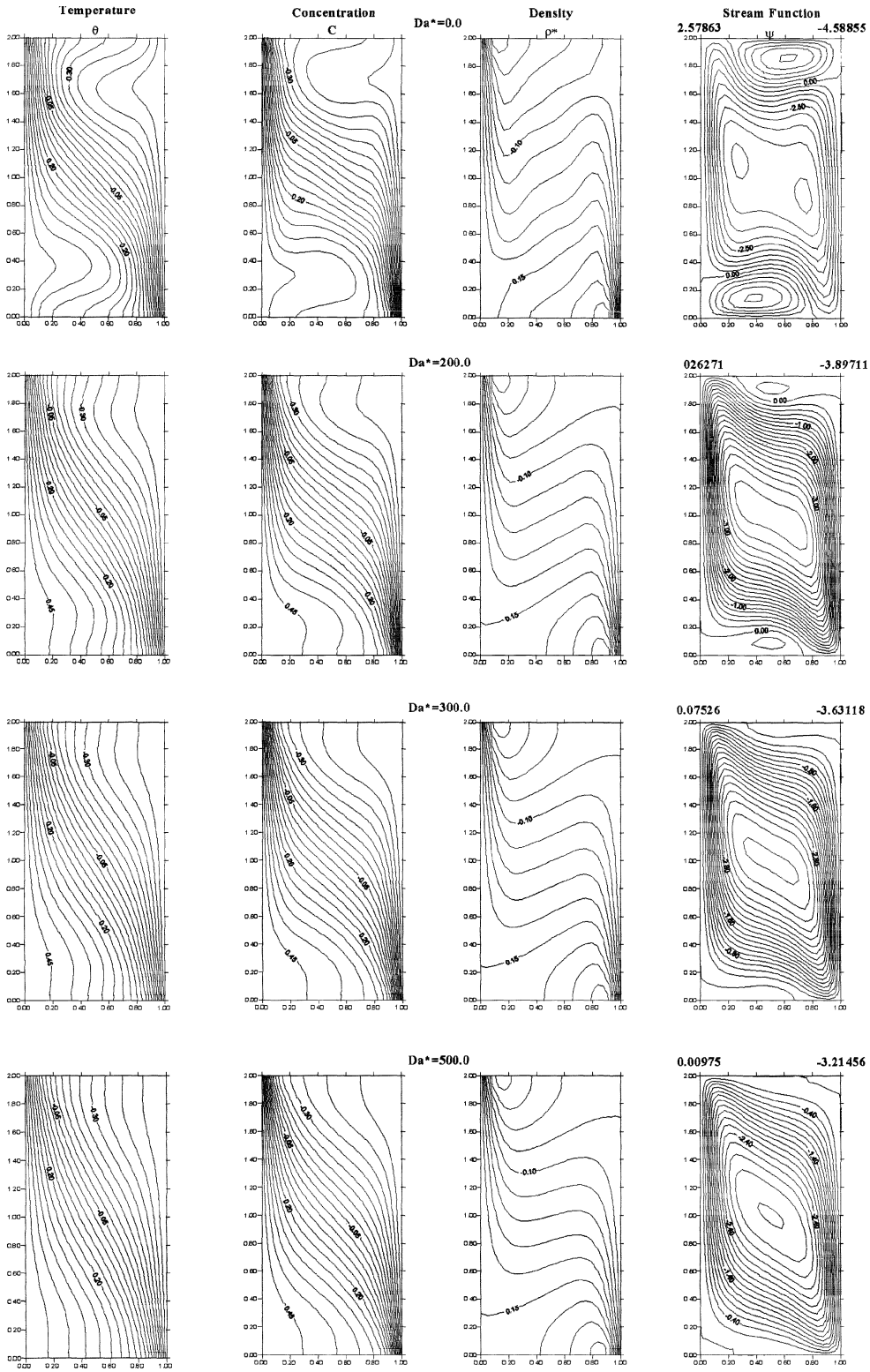


**Figure 8.** Steady thermal-dominated solution for $Le = 2.0$, $N = 1.3$, $Pr = 1.0$, $Ra_T = 10^5$, and $\alpha = 30°$.

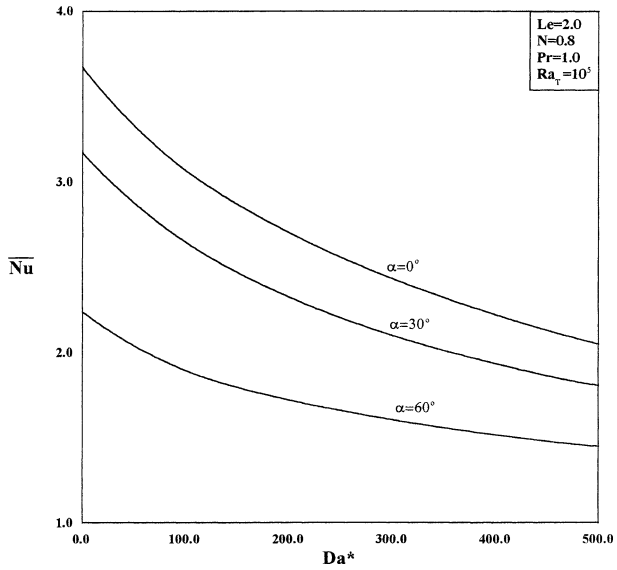


**Figure 9.** Average Nusselt number versus inverse Darcy number for different enclosure angles.

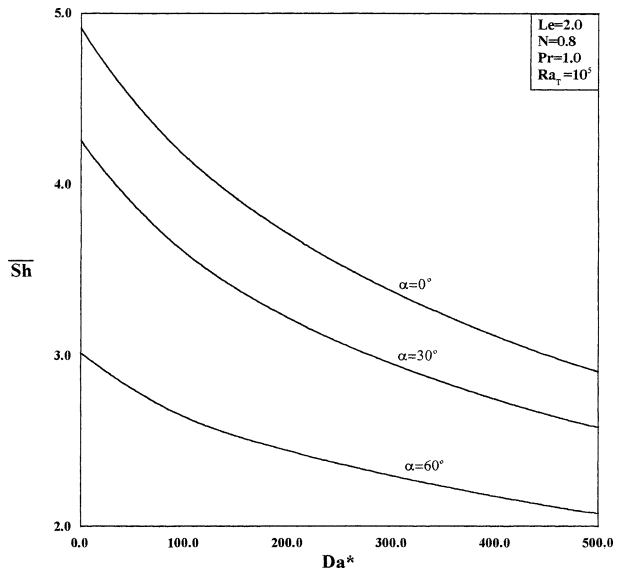


**Figure 10.** Average Sherwood number versus inverse Darcy number for different enclosure angles.

Finally, *figure 15* presents the effects of the presence of the porous medium on the transient oscillatory behavior $|\psi_{\max}|$ and $|\psi_{\min}|$ reported before for $N = 1.0$ in *figure 3*. By comparison with *figure 3*, it is observed that the presence of the porous medium decays the oscillatory behavior in $|\psi_{\max}|$ and $|\psi_{\min}|$ as time progresses.

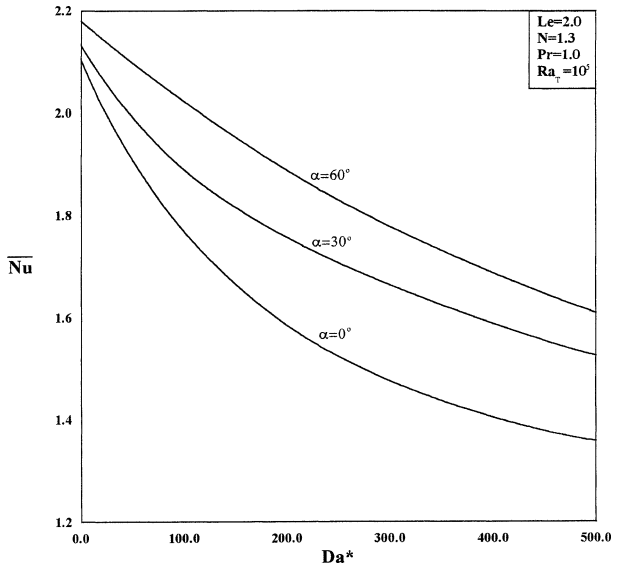


**Figure 11.** Average Nusselt number versus inverse Darcy number for different enclosure angles.

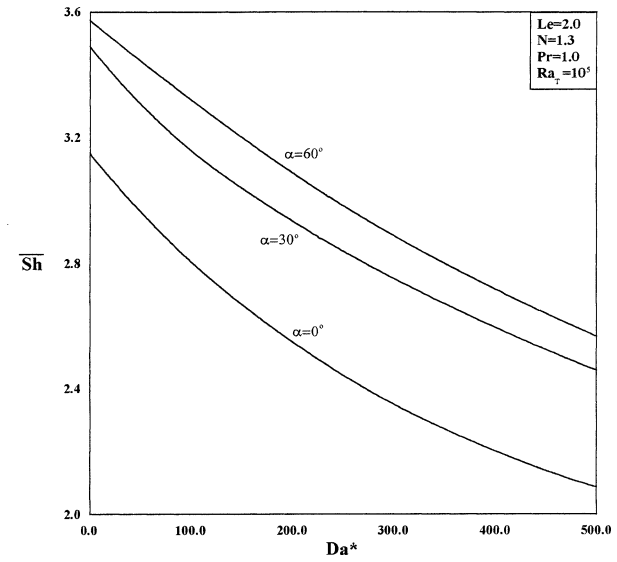


**Figure 12.** Average Sherwood number versus inverse Darcy number for different enclosure angles.

## 7. CONCLUSIONS

The problem of double-diffusive convective flow of a binary mixture inside an inclined rectangular porous enclosure was studied numerically. The finite-difference method was employed for the solution of the present problem. Comparisons with previously published work on special cases of the problem were performed and

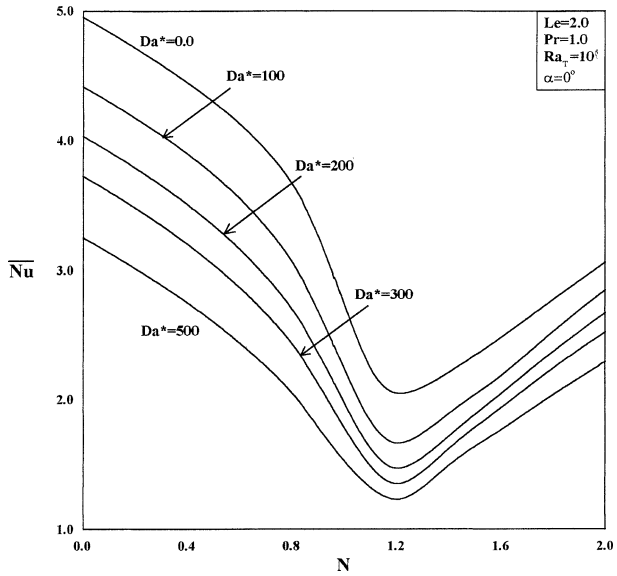


**Figure 13.** Average Nusselt number versus buoyancy ratio for different inverse Darcy numbers.

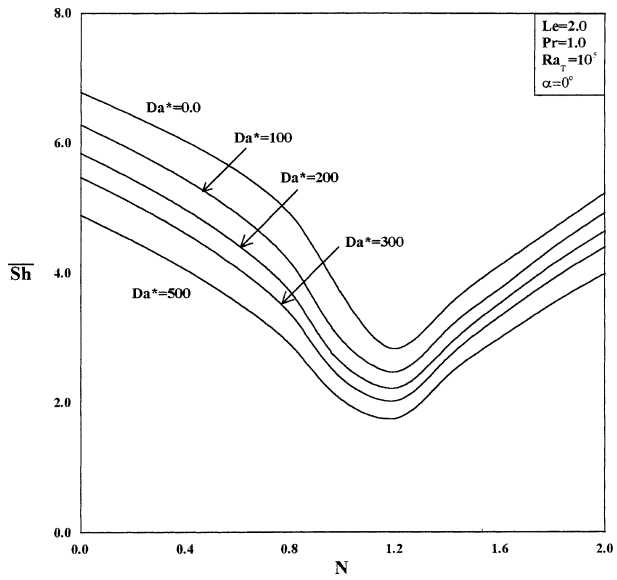


**Figure 14.** Average Sherwood number versus buoyancy ratio for different inverse Darcy numbers.

found to be in good agreement. Graphical results for various parametric conditions were presented and discussed. It was found that the heat and mass transfer mechanisms and the flow characteristics inside the tilted enclosure depended strongly on the inverse Darcy number and the inclination angle. The effect of the presence of the porous medium was found to reduce the heat transfer and the fluid circulation within the enclosure. In addition, it was

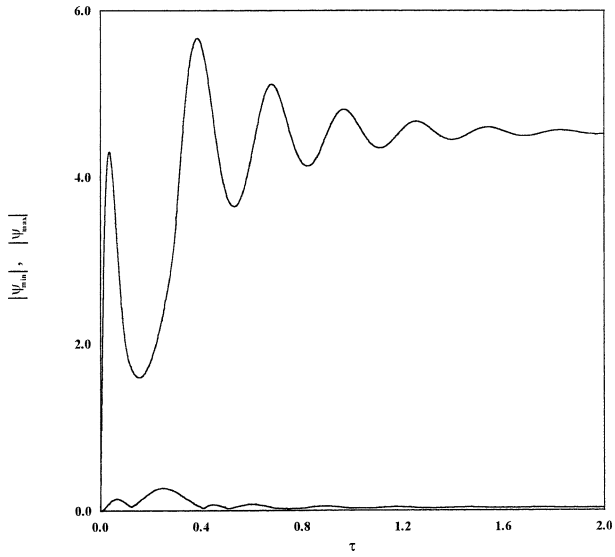


**Figure 15.** Decay of oscillatory behaviour of $|\psi_{\min}|$ and $|\psi_{\max}|$ with time for $Da^* = 500$, $Le = 2.0$, $N = 1.0$, $Pr = 1.0$, $Ra_T = 10^5$, and $\alpha = 0°$.

concluded that there was a critical buoyancy ratio close to 1.2 for which both the average Nusselt and Sherwood numbers were minimum for any value of the inverse Darcy number. The effect of increasing the enclosure inclination angle was found to decrease the average Nusselt and Sherwood numbers for the thermal-buoyancy dominated regime and to increase them for the compositional-buoyancy dominated regime.

## REFERENCES

[1] Beghein C., Haghighat F., Allard F., Numerical study of double-diffusive natural convection in a square cavity, Int. J. Heat Mass Tran. 35 (1992) 833–846.

[2] Ostrach S., Natural convection with combined driving forces, Physicochem. Hydrodyn. 1 (1980) 233–247.

[3] Viskanta R., Bergman T.L., Incropera F.P., Double-diffusive natural convection, in: Kakac S., Aung W., Viskanta R. (Eds.), Natural Convection: Fundamentals and Applications, Hemisphere, Washington, DC, 1985, pp. 1075–1099.

[4] Bejan A., Mass and heat transfer by natural convection in a vertical cavity, Int. J. Heat Fluid Flow 6 (1985) 149–159.

[5] Kamotani Y., Wang L.W., Ostrach S., Jiang H.D., Experimental study of natural convection in shallow enclosures with horizontal temperature and concentration gradients, Int. J. Heat Mass Tran. 28 (1985) 165–173.

[6] Ostrach S., Jiang H.D., Kamotani Y., Thermo-solutal convection in shallow enclosures, in: ASME-JSME Thermal Engrg. Joint Conf., Hawaii, 1987.

[7] Lee J., Hyun M.T., Kim K.W., Natural convection in confined fluids with combined horizontal temperature and

concentration gradients, Int. J. Heat Mass Tran. 31 (1988) 1969–1977.

[8] Lee J.W., Hyun J.M., Double-diffusive convection in a rectangle with opposing horizontal and concentration gradients, Int. J. Heat Mass Tran. 33 (1990) 1619–1632.

[9] Hyun J.M., Lee J.W., Double-diffusive convection in a rectangle with cooperating horizontal gradients of temperature and concentration gradients, Int. J. Heat Mass Tran. 33 (1990) 1605–1617.

[10] Mamou M., Vasseur P., Bilgen E., Analytical and numerical study of double diffusive convection in a vertical enclosure, Heat Mass Tran. 32 (1996) 115–125.

[11] Mamou M., Vasseur P., Hysteresis effect on thermosolutal convection with opposed buoyancy forces in inclined enclosures, Int. Comm. Heat Mass Tran. 26 (1999) 421–430.

[12] Ranganathan P., Viskanta R., Natural convection of a binary gas in rectangular cavities, in: ASME-JSME Thermal Engrg. Joint Conf., Hawaii, 1987.

[13] Trevisan O.V., Bejan A., Combined heat and mass transfer by natural convection in a vertical enclosure, ASME J. Heat Tran. 109 (1987) 104–112.

[14] Nishimura T., Wakamatsu M., Morega A.M., Oscillatory double-diffusive convection in a rectangular enclosure with combined horizontal temperature and concentration gradients, Int. J. Heat Mass Tran. 41 (1998) 1601–1611.

[15] Mamou M., Vasseur P., Bilgen E., A Galerkin finite-element study of the onset of double-diffusive convection in an inclined porous enclosure, Int. J. Heat Mass Tran. 41 (1998) 1513–1529.

[16] Chen F., Chen C., Double-diffusive fingering convection in a porous medium, J. Heat Tran. 36 (1993) 793–897.

[17] Trevisan O.V., Bejan A., Mass and heat transfer by natural convection in a vertical slot filled with porous medium, Int. J. Heat Mass Tran. 29 (1986) 403–415.

[18] Alavyoon F., On natural convection in vertical porous enclosures due to prescribed fluxes of heat and mass at the vertical boundaries, Int. J. Heat Mass Tran. 36 (1993) 2479–2498.

[19] Mamou M., Vasseur P., Bilgen E., Gobin D., Double diffusive convection in an inclined slot filled with porous medium, European Journal of Mechanics/Fluids 14 (1995) 629–652.

[20] Lin D., Unsteady natural convection heat and mass transfer in a saturated porous enclosure, Wärme und Stoffübertragung 28 (1993) 49–56.

[21] Alavyoon F., Masuda Y., On natural convection in vertical porous enclosures due to opposing fluxes of heat and mass prescribed at the vertical walls, Int. J. Heat Mass Tran. 37 (1994) 195–206.

[22] Mamou M., Vasseur P., Bilgen E., Double-diffusive convection instability in a vertical porous enclosure, J. Fluid Mech. 386 (1998) 263–289.

[23] Amahmid A., Hasnaoui M., Vasseur P., Boundary layer flows in a vertical porous enclosure induced by opposing buoyancy forces, Int. J. Heat Mass Tran. 42 (1999) 3599–3608.

[24] Bennacer R., Beji H., Vasseur P., The Brinkman model for thermosolutal convection in a vertical annular porous layer, Int. Comm. Heat Mass Tran. 27 (2000) 69–80.

[25] Morega A.M., Nishimura T., Double-diffusive convection by Chebyshev collocation method, Technology Reports of the Yamaguchi University 5 (1996) 259–276.